Microchimica Acta (2021) 188: 53
https://doi.org/10.1007/s00604-021-04710-7

ORIGINAL PAPER

Determination of β-amyloid oligomer using electrochemiluminescent aptasensor with signal enhancement by AuNP/MOF nanocomposite

Lixiu Yin[1] · Yueju Wang[2] · Rong Tan[1] · Huiling Li[2] · Yifeng Tu[1]

Received: 21 October 2020 / Accepted: 10 January 2021 / Published online: 26 January 2021

Abstract

In order to effectively and conveniently detect the β-amyloid oligomer (AβO) for earlier diagnosis of Alzheimer's disease (AD), a disposable aptamer biosensor has been developed with high performance, facile operation, and low cost. Using a nanocomposite by in situ reduction of chloroauric acid to decorate Au nanoparticles (AuNPs) on Fe-MIL-88NH$_2$ material via Au–N bond to effectively enhance the electrochemiluminescence (ECL) of luminol, the functioned basal electrode provides adequate background for sensing response. When the aptamer is linked via Au–S bond on the surface, the sensor gets the ability of specific recognition and coalescence toward the target (AβO). After incubating the sample on the aptasensor, its ECL signal is inhibited owing to the steric hindrance of the AβO macromolecules. The relative inhibition ratio linearly depends to the logarithm of AβO concentration in the range 0.1 pM to 10 pM, with an LOD of 71 fM. The aptasensor has high selectivity to AβO among its analogs. The recoveries in human serum were 98.9–105.4%. This research provides a new approach for sensitive detection of AβO in clinic laboratories for investigation and diagnosis of AD.

Keywords β-Amyloid oligomer · Alzheimer's disease · Electrochemiluminescence · Aptasensor · AuNPs/Fe-MOF nanocomposite

Introduction

Alzheimer's disease (AD) is a kind of very terrible neurodegenerative disease, which brings in seriously physiological and psychological trauma to patients and their families [1]. So far, after the worldwide research for half-century, only a sole aducanumab drug is approved by FDA of the USA for clinical therapy of AD in 2020 [2]. The effect of this drug is to eliminate those β-amyloid proteins by immune interaction from the brain of those patients with mild dementia or early signs, to alleviate the further worse of AD. This milestone marks the rationality of those researches on relationship between β-amyloid protein and AD. As we know, the studies have shown that the β-amyloid oligomer (AβO) with 42 amino acids ($A\beta_{1-42}$) has most neurotoxic effect on nerve system [3]. As a precursor, ascending to greater than 36 pM of content in serum of mild dementia [4], it closely correlated with the deposition of β-amyloid protein as fibers in the brain. Thus, it is a tremendous challenge to explore better methods for β-amyloid oligomer detection in human blood/serum samples quickly and sensitively in the early stage of AD [5, 6].

Several methods have been introduced to detect Aβ oligomer in body fluid; among them, the enzyme-linked immunosorbent assay (ELISA) is the commonest used method [7] besides fluorescent [8] or electrochemical ones [9] with nice performance and practicability. However, as for ELISA, using peptide or antibody as recognition host to ensure the specificity is expensive and time-consuming; meanwhile, other methods are deficient in sensitivity [10, 11]. Therefore, it is worthy of exploration to develop more sensitive and precise method with less time consumption and low cost for AβO detection.

Aptamer, a short single-stranded DNA or RNA biomolecule obtained by screening in vitro using the way of systematic evolution of ligands by exponential enrichment (SELEX) [12], is a

✉ Huiling Li
lhl8543@126.com

✉ Yifeng Tu
tuyf@suda.edu.cn

[1] College of Chemistry, Chemical Engineering and Material Science, Soochow University, Suzhou 215123, People's Republic of China

[2] First Affiliated Hospital of Soochow University, Suzhou 215006, People's Republic of China

better choice for specifically molecular recognition in biosensing. It is easy to be synthesized and modified and is non-immunogenic and inexpensive (under a tenth of antibody), used in various fields as fluorescence, electrochemistry, and electrochemiluminescence (ECL) as the successor of antibodies [13, 14]. Of course, the upsurging clinical use of aptamers is still on road. The affinity of aptamer toward target is not as high as that of antibody yet account of that the artificial process of SELEX was still not enough to rival immune system, and the specificity of aptamers to unknown human proteins is somewhat worried. However, it is certainly believable, experienced 20 years of study by the biomedical community, that the future of practically clinical diagnosis based on aptamers is not a dream [15].

Studies have also shown that the nanomaterials can significantly reduce the detection limit for several orders of magnitude [16]. Metal-organic frameworks (MOFs) are the porous crystal similar to zeolite [17]. They have diverse and adjustable crystalline porous structure [18], which brought in better thermostability and chemical stability, high superficial area [19], high activity with dense active spot [20], and high and durable catalytic performance [21]. They can be used as ideal supporter for biomolecules and perspective catalyst for biosensors with good biocompatibility [22, 23]. More interestingly, the conductivity and catalysis of MOFs can be further improved by nanodoping for several orders of magnitude [24], such as to use metal nanoparticles. Among them, Au nanoparticles (AuNPs) are widely used in the preparation of biosensors due to its excellent conductivity and electrocatalytic properties [24]. The association of AuNPs on MOFs crystal can not only effectively prevent the aggregation of metal nanoparticles [25] but also improve the conductivity, stability, and catalytic activity of the composite [22]. Recently, it has been found that Fe-MIL-88NH_2 can load a large amount of AuNPs to act as a carrier in the preparation of various biosensors.

A new aptasensor using AuNPs/Fe-MIL-88NH_2 as substrate and sensitizing material will be reported in this paper. Functionalized Fe-MOFs with AuNPs (AuNPs/Fe-MOFs) was attached onto the surface of indium tin oxide (ITO)–coated glass via Au–N bonds to act as sensor substrate in assistance with APTMS, then caught aptamer molecules by Au–S bond. After the specifically binding of Aβ oligomer with the aptamer, the ECL output of the sensor is suppressed owing to the steric hindrance of this complex toward the ECL probe. With luminol as a luminescent reporter to quantitatively detect the concentration of Aβ oligomer, the ECL sensor reaches a detection limit of 71.0 fM.

Experimental

Materials

The specific DNA aptamer of AβO (5′-HS-GCCTGTGT TGGGGCGGGTGCG) is purchased from Sangon Biotech. Co., Ltd. (Shanghai, P. R. China). Human Aβ (1–42) is purchased from Dalian Meilun Biotechnology Co. Ltd. (Dalian, P. R. China). Luminol is obtained from Fluka Chem. Co. (USA). Bovine serum albumin (BSA) and $NaHPO_4$ and Na_2HPO_4 are provided by Sinoparm Chemical Reagent Co., Ltd. (Shanghai, P. R. China). 3-Aminopropyltrimethoxysilane (APTMS) is provided by Aladdin-Reagent Co., Ltd. (Shanghai, P. R. China). Human AβO (1–42) ELISA kit is provided by Ruifan Tech. Co. Ltd. (Shanghai P. R. China). Blood samples are collected in the First Affiliated Hospital of Soochow University. Chemicals are all analytical grade and ultrapure water (18.2 MΩ cm) is used in experiments. Indium tin oxide (ITO)–coated glass, purchased from Guluo Glass Electronics Co, Ltd. (Luoyang, P. R. China), was cut into 5.0 cm × 1.0 cm pieces for use.

Instruments

Electrochemiluminescence tests were carried out on a lab-built equipment with PMT as luminescence detector; the details are described in Section 1 in Electronic Supporting Material (ESM). The concentration of Aβ (1–42) standard solution was calibrated by NANODROP 2000 Microvolume UV-Vis Spectrophotometer (Thermo Scientific, USA). The distribution and element content of nanomaterials were characterized by S-4700 Scanning Electron Microscope (SEM) coupled with X-ray energy spectrum analysis (EDS) (Hitachi, Japan). The morphology and size of nanomaterials are observed by Tecnai G20 Transmission Electron Microscope (TEM) (FEI, USA). The infrared spectroscopy is recorded using Nicolet 6700 FT-IR spectrometer (Thermo Nicolet, USA) to show the structural character of material. The crystals were characterized using D2 Paser X-Ray Diffractometer (XRD, Bruker, Germany) with a Cu target (Kα, λ = 1.542 Å). Electrochemical impedance spectroscopy (EIS) and cyclic voltammetry (CV) were measured using an RST-5200 electrochemical workstation (Risetest Instruments Co. Ltd. Suzhou, P. R. China).

Preparation of Fe-MIL-88NH_2 and AuNPs/Fe-MOFs

Referring to previous reports [17, 19], the Fe-MIL-88NH_2 and AuNPs/Fe-MOFs have been synthesized with slight modification. The details are presented in Section 2 in ESM.

Preparation of AβO aptasensor

As shown in Scheme 1, ITO glass was cleaned with ethanol/water (1:1) solution of sodium hydroxide and 50% acetone solution successively, and then hydroxylated overnight in 30% ammonia. After dried with a nitrogen

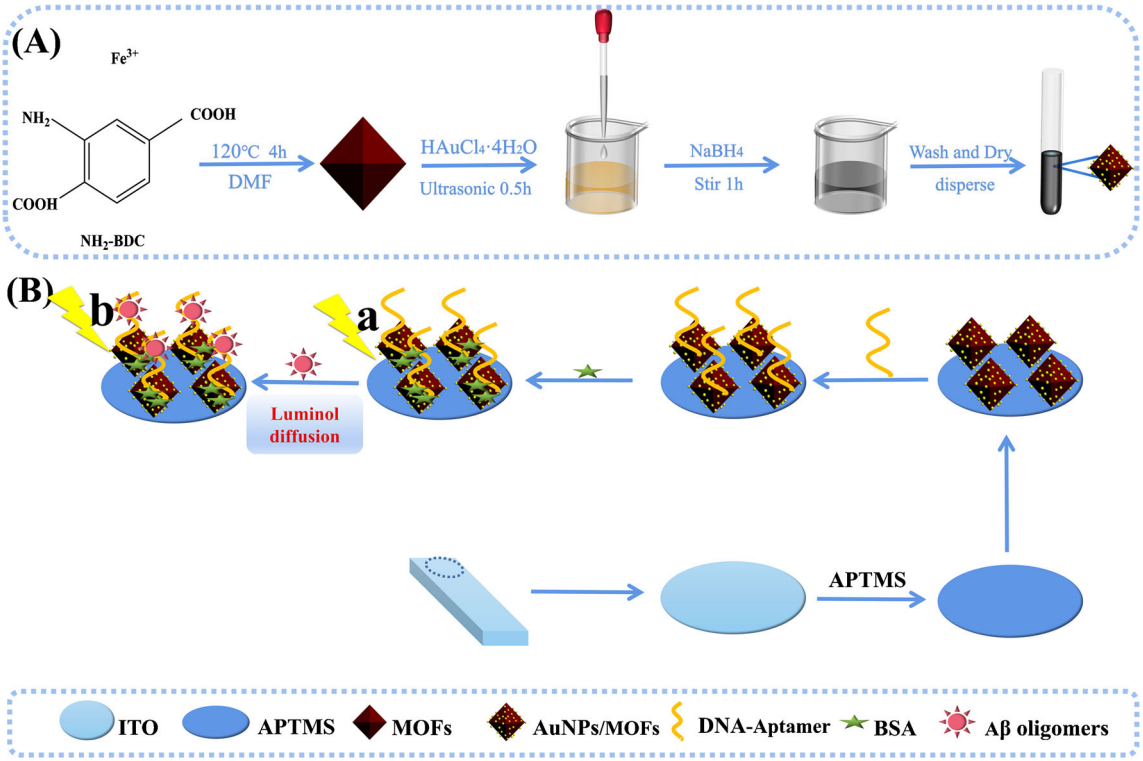

Scheme 1 The fabrication procedure and sensing mechanism of the ECL aptasensor

stream, 10 μL of 0.03% (*V*/*V*) anhydrous ethanol solution of APTMS was rapidly dripped onto its surface under the condition of humidity less than 20%. Volatile clean the ethanol in a dryer for 1 h, the APTMS was hydrolyzed at 55 °C with saturated humidity for 4 h to get a thin layer of silicon rubber. Fifty microliters of previously prepared AuNPs/Fe-MOFs dispersion was dropped on this surface and let it stood for 2 h at room temperature to ensure the firmly Au–N binding. Then, rinsed off those excess materials with ultrapure water and followed by nitrogen blow-drying. The aptamer (10 μL, 5 μM) was incubated on this function matrix for 9 h at 4 °C, to be tightly combined via Au–S bond to endow the ability of aptasensing. Finally, adequate 1% BSA solution was used to block the residual active sites, incubated at 25 °C for 2 h. The unbound maters were then washed away with ultrapure water. The prepared sensor is stored at 4 °C for further use.

Detection of AβO employing prepared aptasensor

The supporting electrolyte is phosphate buffer (5 mL, pH = 8.0) containing 1.0×10^{-5} M luminol. A three-electrode system (a silver stick as reference electrode, a platinum wire as auxiliary electrode, and developed aptasensor as working electrode) was used for ECL measurement. Every 10 μL of AβO samples was dripped on the sensor surface and incubated for 1.5 h at 37 °C in advance.

Results and discussion

The sensing mechanism of developed ECL aptasensor

The sensing mechanism of developed ECL aptasensor is illustrated in Scheme 1. Profit from the gelation of ITO surface with APTMS, the AuNPs/Fe-MOFs were decorated on it via Au–N bond, then was used as the base electrode. With luminol as a luminescent probe, its anion is oxidized to form the free radical under applied high potential, then produced 3-aminophthalate exciton [26]. Taking turns at low potential, the yielded reactive oxygen species (ROSs, such as superoxide radical $^{\cdot}O$, hydrogen peroxide H_2O_2, and hydroxyl radical $^{\cdot}OH$) greatly promoted the excitation of luminol by energy transfer [27] (displayed in Scheme S1, ESM). Compared with bare ITO, the decoration of AuNPs/Fe-MOFs significantly enhances this process. This might be owing to the catalytic effect of nanomaterials on yielding of oxygen free radicals and extended duration between ROSs and luminol anion free radical [28]. Here, the AuNPs are favorite for the sensing ability of biosensors since the excellent conductivity [29] also provides more active sites for aptamer linkage by the Au–S bond. The MOF material acts as a good substrate for burdening AuNPs, thereafter, to improve the biocompatibility of the surface for those biomolecules [30]. After that, the aptamer was firmly bound on the AuNPs via sulfydryl, and then block those nonspecific sites with BSA. Therefore, the output signal on the sensor is regarded as the background (noted as "a").

After it happened of the specific combination of oligomer with aptamer, degree of steric hindrance for probe approaching occurred, resulting in declined signal (noted as "b"). The relative value ($\Delta I/I = (a-b)/a$) can be employed for quantitative detection.

The characterization of Fe-MOFs and AuNPs/Fe-MOFs

As shown in Fig. 1a, the transmission electron microscope (TEM) revealed the morphology of Fe-MIL-88NH_2. Consistent with previous report [17], Fe-MIL-88NH_2 presents a morphology of typical regular octahedral crystal with the diameter of about 150 nm. When Au was deposited on, it has practically covered the MOFs (inset in Fig. 1a). It can also be clearly seen in SEM images (Fig. 1b, c), there are flowering twig Au particles with the size of 10 nm high densely piled on Fe-MOFs. Meanwhile, the EDS (Fig. S3) determined the ratio of Au to Fe as 3.8, further supporting the verdict. The X-ray diffraction (XRD) is used to check the crystal structure of the synthesized MOF and AuNPs/Fe-MOF composite. The diffraction peaks at 9.03°, 10.4°, and 16.4° (as displayed in Fig. 1d) for (002), (101), and (103) faces on XRD spectrum of Fe-MIL-88NH_2 totally conform to the typical data in reported literature [31]. While in the disappearance of those XRD peaks of MOFs, new peaks of mono-metal phase Au appeared (as shown in Fig. 1e). Four characteristic peaks of gold appeared at 38.18°, 44.4°, 64.58°, and 77.55° perfectly matched the (111), (200), (220), and (311) faces of Au crystal [22]. These results also demonstrate the dense overlap of nanosized Au crystals on Fe-MOFs, which isolated the XRD signal of MOFs. The interaction between MOFs and Au can be verified by IR spectroscopy (as shown in Fig. S4). Obviously, compared to NH_2-H_2BDC (curve a), the disappearance of the wide peak of -OH around 3050 cm^{-1} in Fe-MOFs (curve b) indicates the coordination between -COOH and Fe^{3+}. Meanwhile, the blue shift (from 1688 to 1584 cm^{-1}, 1421 to 1378 cm^{-1}) of stretching vibration of carbonyl C–H in benzene ring also proves it, due to the weakened negative induction effect. On IR curve of AuNPs/Fe-MOFs (curve c), the characteristic peaks of primary amine at 3486 and 3372 cm^{-1} in curve b are vanished and left only one single peak at 3448 cm^{-1}, indicating the interaction between AuNPs and Fe-MOFs via Au–N bond.

Figure 2a and b show the dependence of CV currents upon scan rates on bare ITO and nanofunctioned electrode with an electroactive probe $Fe(CN)_6^{4-/3-}$. The linear diagrams (Fig. 2c, d) are acquired between I_p and $\nu^{1/2}$, totally in accordance with Randles-Sevcik equation ($I_p = 2.69 \times 10^5 n^{3/2} A D^{1/2} C \nu^{1/2}$, where I_p for peak current (A), n for electron transfer number, A for electrode area (cm^2), D for diffusion coefficient (cm^2/s), C for concentration (mol/cm^3), and ν for scan rate (V/s)). The results inferred that the nanofunction of electrode did not alter the mechanism of electrochemical reaction; it is still a diffusion controlled one. Thus, the effective area of nanofunctioned electrode is 1.47 time of bare ITO electrode, suggesting a better result than previously reported AuNP-modified electrode [32].

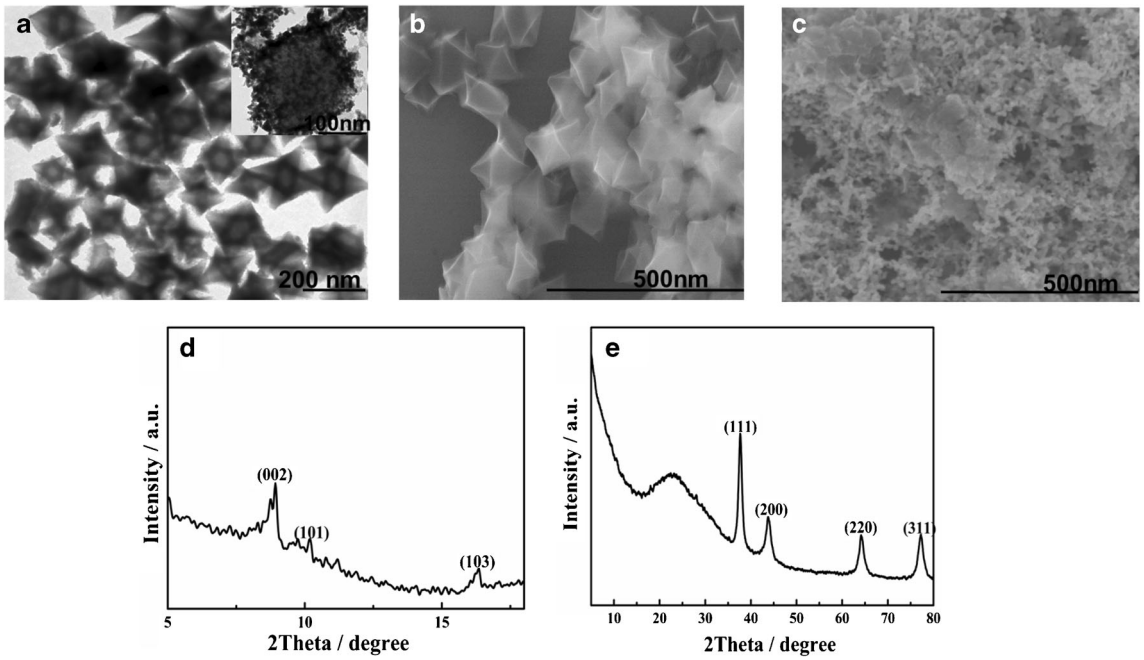

Fig. 1 **a** The TEM images of Fe-MOFs and AuNPs/Fe-MOFs (inserted). The SEM image of **b** Fe-MOFs and **c** AuNPs/Fe-MOFs. The X-ray diffraction patterns of **d** Fe-MIL-88NH_2 and **e** AuNPs/Fe-MOFs

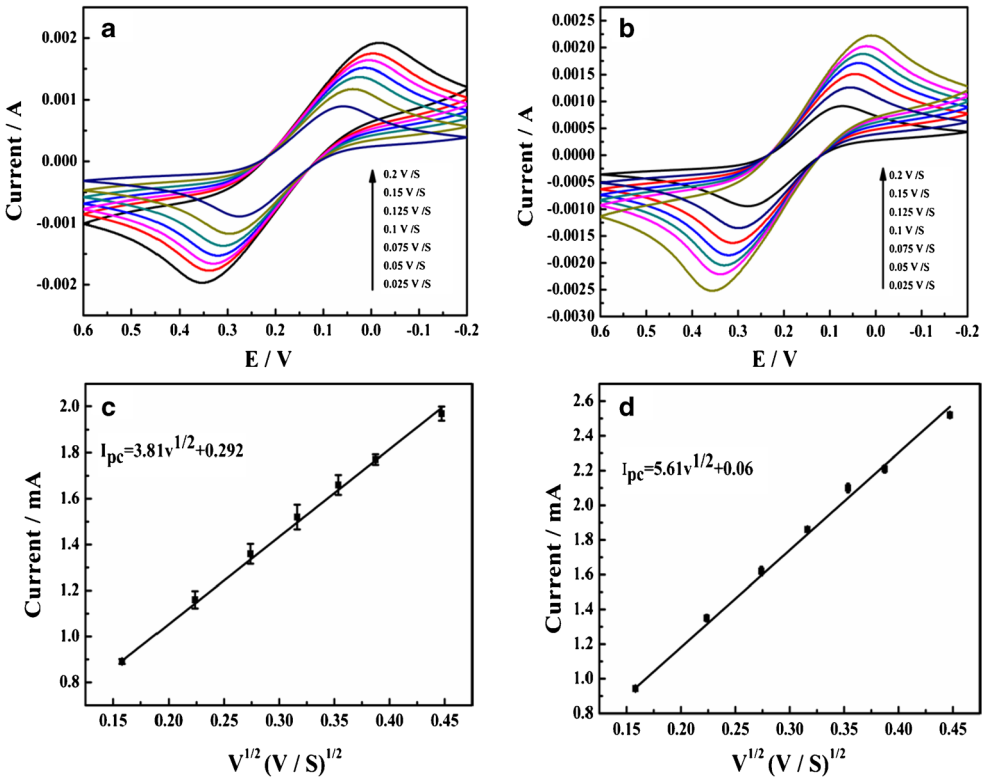

Fig. 2 The CVs of **a** bare ITO and **b** AuNPs/Fe-MOFs/ITO in 0.1 M KCl solution containing 5 mM Fe $(CN)_6^{3-/4-}$ at different scanning rate; correspondingly, the **c** and **d** are the liner relationship of peak currents vs. $\nu^{1/2}$

Optimization of aptasensor performance

The details for optimization of nanofunction electrode are described in ESM (Fig. S5). Under these conditions, compared with simply using AuNPs (sized about 15–20 nm), the nanocomposite functioned electrode shows better ECL performance (as shown in Fig. S6). Some comparison about the performance of MOF-based ECL sensors is shown in Table S1; it can be found that the AuNPs/Fe-MOFs were excellent both in terms of sensitivity and cost. Those conditions for aptasensor performance are also optimized (see detailed discussion in ESM, Section 3).

Analytical performance of the aptasensor

The electrochemical behavior of the electrode was demonstrated by cyclic voltammetry and electrochemical impedance spectroscopy, conducted in a 0.1 M KCl solution containing 5 mM $Fe(CN)_6^{3-}$. The peak current of CV is lower than that of ITO after the coverage of APTMS, but increases significantly if functioned with nanocomposite (as shown in Fig. 3a (a, b, c)). After the biomolecules were immobilized on, the peak current decreased gradually, indicating the successful preparation of the sensor (curves d, e, and f). The

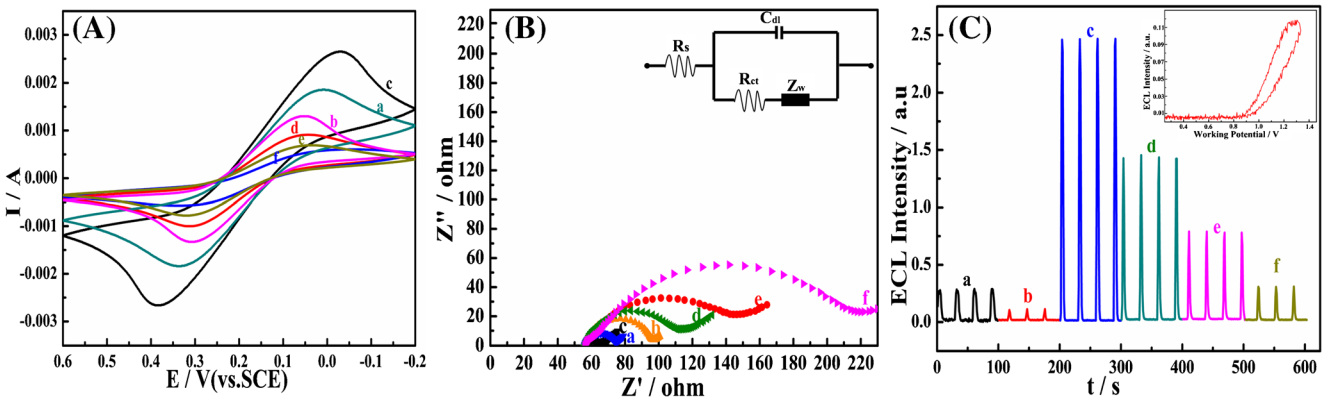

Fig. 3 The **a** CVs (under scanning rate of 50 mV s^{-1}) and **b** EIS of (a) ITO, (b) APTMS/ITO, (c) AuNPs/Fe-MOFs/ITO, (d) aptamer/AuNPs/Fe-MOFs/ITO, (e) resultant sensor, and (f) after binding with AβO, in 0.1 M KCl solution containing 5 mM Fe $(CN)_6^{3-/4-}$. **c** The ECL maps of those electrodes in 1×10^{-5} M luminol solution (phosphate buffer, pH 8.0), inserted is the ECL signal during CV scan

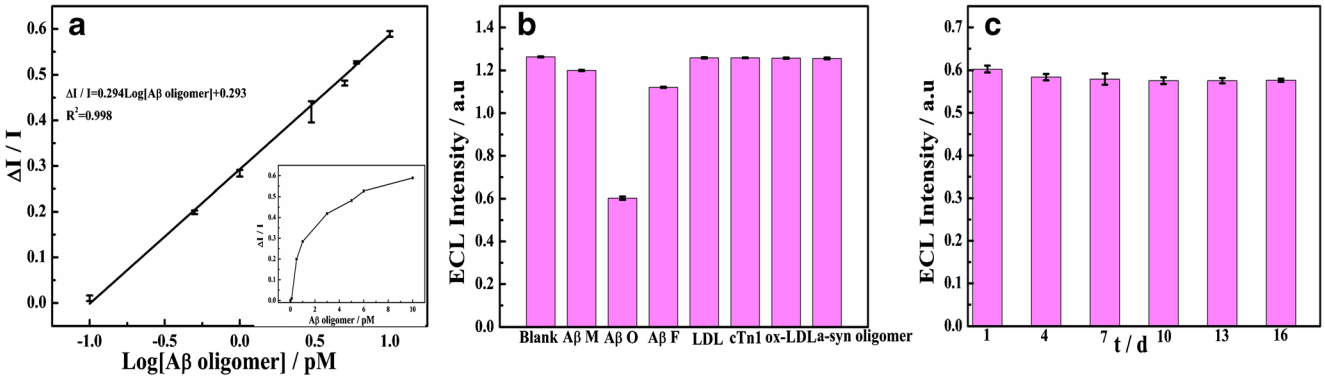

Fig. 4 **a** The linear regression of relative inhibition ratio of ECL sensing signal upon the logarithm of AβO concentration, inserted is the ECL sensing output of the sensor upon AβO concentration. **b** The check results of potential interference of different substances on the sensor. **c** The stability of the sensor during 16 days

EIS info (Fig. 3b) also support this conclusion, these changes in turn indicated the performance of ITO, APTMS, AuNPs/Fe-MOFs, aptamer, bovine serum albumin, and oligomer. The ECL signal of the sensor is also well consistent with these results (Fig. 3c).

Under abovementioned optimal conditions, the differently concentrated oligomer was detected, as gradually declined ECL sensing output. The results showed a linear regression of inhibition ratio of ECL signal upon the logarithm of oligomer concentration with the equation $\Delta I/I = 0.294 \log [A\beta O] + 0.293$ ($R^2 = 0.998$) (see Fig. 4A) ranged in 0.1 to 10 pM, and the detection limit is 71.0 fM (LOD = 3*S*/*N*, *n* = 7). Table S2 in ESM makes a comparison of this sensor with other methods, which evidences its lower detection limit and higher sensitivity.

To verify the specificity of the aptasensor and its practicability in real sample detection, the latent effect of common coexisting substances was checked. With 10 nM of cTn1, α-syn oligomer, Aβ monomer, and Aβ fiber, 1 M of LDL, and ox-LDL against 10 pM of Aβ oligomer, as can be seen from Fig. 4b, only the Aβ monomer and Aβ fiber slightly disturbed the detection. This must be owing to the high specific binding of the aptamer with Aβ oligomer (the dissociation constant is 25 nM [33]). The reproducibility and stability, as principal performances of the sensor, should be taken into account in practical use. Five parallel sensors were tested to detect the AβO of 10 pM; a fine reproducibility with 3.23% of RSD was testified. The prepared sensors were stayed for 16 days; no significant change was found (see Fig. 4c).

Table 1 Detection results of AβO in real samples using aptasensor and ELISA kit

Sample no.	AβO in sample (pM)	
	This method	ELISA
1	41	38
2	45	37
3	50	43

Application of the developed aptasensor

According to previous reports [34], the concentration of AβO in serum is positively correlated with cerebrospinal fluid. In order to verify the clinical applicability of the developed aptasensor, several samples from hospital who have certain symptoms of AD were determined and compared the results with the commercial ELISA method. The samples were diluted for tenfolds with 10 mM buffer solution (pH = 7.4), then dropped a 10-μL portion onto the aptasensor for incubation at 37 °C for 1.5 h; the ECL signal was then measured. The results are listed in Table 1, principally accord with ELISA. The recoveries are listed in Table 2, in the range of 98.9–105.4%, means a good accuracy.

Conclusion

In conclusion, an aptasensor was developed based on the ECL signaling of luminol for Aβ oligomer detection, using AuNPs/Fe-MOF nanocomposite as the sensitizing material. The aptasensor has high sensitivity, which makes precise

Table 2 The recoveries of the AβO detection in real samples

Sample no.	AβO in sample (pM)	Added (pM)	Found (pM)	Recovery (%)	RSD (%, *n*=5)
1*	0.407	0.2	0.612	102.5	2.46
		0.5	0.934	105.4	1.88
		1	1.396	98.9	1.67

*The sample is collected from a healthy volunteer

quantification of AβO with an LOD as low as 71 fM. Compared with other methods for AβO detection (such as fluorescence analysis, ELISA, and electrochemical methods), it has advantages of simple operation, short analysis time, and low cost since the sensing components used in this sensor need not to be labeled. The prepared aptasensor may potentially become a feasible alternative method for simple and sensitive clinical assay as "liquid biopsy" of Aβ species related to AD diagnosis.

Supplementary Information The online version contains supplementary material available at https://doi.org/10.1007/s00604-021-04710-7.

Funding This work is financially supported by the National Natural Science Foundation of China (21675115, 21375091).

Compliance with ethical standards All procedures performed in studies involving human participants were in accordance with the ethical standards of the institutional research committee and with the 1964 Helsinki declaration and its later amendments or comparable ethical standards. Protocol number: 2019(264), the First Affiliated Hospital of Soochow University.

Conflict of interest The authors declare that they have no competing interests.

References

1. Zhu H, Zhou P, Alcauter S, Chen Y, Cao H, Tian M, Ming D, Qi H, Wang X, Zhao X, He F, Ni H, Gao W (2016) Changes of intranetwork and internetwork functional connectivity in Alzheimer's disease and mild cognitive impairment. J Neural Eng 13(4):046008. https://doi.org/10.1088/1741-2560/13/4/046008
2. Vaz M, Silvestre S (2020) Alzheimer's disease: recent treatment strategies. Eur J Pharmacol 887:173554. https://doi.org/10.1016/j.ejphar.2020.173554
3. Auld DS, Kornecook TJ, Bastianetto S, Quirion R (2002) Alzheimer's disease and the basal forebrain cholinergic system: relations to β-amyloid peptides, cognition, and treatment strategies. Prog Neurobiol 68(3):209–245. https://doi.org/10.1016/S0301-0082(02)00079-5
4. Klaver AC, Coffey MP, Smith LM, Bennett DA, Finke JM, Dang L, Loeffler DA (2011) ELISA measurement of specific non-antigen-bound antibodies to Aβ1-42 monomer and soluble oligomers in sera from Alzheimer's disease, mild cognitively impaired, and noncognitively impaired subjects. J Neuroinflammation 8(1):93. https://doi.org/10.1186/1742-2094-8-93
5. Zhao G, Wang Y, Li X, Yue Q, Dong X, Du B, Cao W, Wei Q (2019) Dual-quenching electrochemiluminescence strategy based on three-dimensional metal–organic frameworks for ultrasensitive detection of amyloid-β. Anal Chem 91(3):1989–1996. https://doi.org/10.1021/acs.analchem.8b04332
6. Deng C, Liu H, Si S, Zhu X, Tu Q, Jin Y, Xiang J (2020) An electrochemical aptasensor for amyloid-β oligomer based on double-stranded DNA as "conductive spring". Microchim Acta 187(4):239. https://doi.org/10.1007/s00604-020-4217-8
7. Xia N, Liu L, Harrington MG, Wang J, Zhou F (2010) Regenerable and simultaneous surface plasmon resonance detection of Aβ(1−40) and Aβ(1−42) peptides in cerebrospinal fluids with signal amplification by streptavidin conjugated to an N-terminus-specific antibody. Anal Chem 82(24):10151-10157. https://doi.org/10.1021/ac102257m
8. Liu L, Chang Y, Yu J, Jiang M, Xia N (2017) Two-in-one polydopamine nanospheres for fluorescent determination of beta-amyloid oligomers and inhibition of beta-amyloid aggregation. Sensors Actuators B: Chem 251:359-365. https://doi.org/10.1016/j.snb.2017.05.106
9. Negahdary M, Heli H (2019) An ultrasensitive electrochemical aptasensor for early diagnosis of Alzheimer's disease, using a fern leaves-like gold nanostructure. Talanta 198:510-517. https://doi.org/10.1016/j.talanta.2019.01.109
10. Zhu L, Zhang J, Wang F, Wang Y, Lu L, Feng C, Xu Z, Zhang W (2016) Selective amyloid β oligomer assay based on abasic site-containing molecular beacon and enzyme-free amplification. Biosensors and Bioelectronics 78:206-212. https://doi.org/10.1016/j.bios.2015.11.048
11. Zhou J, Meng L, Ye W, Wang Q, Geng S, Sun C (2018) A sensitive detection assay based on signal amplification technology for Alzheimer's disease's early biomarker in exosome. Anal Chim Acta 1022:124-130. https://doi.org/10.1016/j.aca.2018.03.016
12. Zhou Y, Zhang H, Liu L, Li C, Chang Z, Zhu X, Ye B, Xu M (2016) Fabrication of an antibody-aptamer sandwich assay for electrochemical evaluation of levels of β-amyloid oligomers. Sci Rep 6(1):35186. https://doi.org/10.1038/srep35186
13. Jiang L-F, Chen B-C, Chen B, Li X-J, Liao H-L, Huang H-M, Guo Z-J, Zhang W-Y, Wu L (2017) Detection of Aβ oligomers based on magnetic-field-assisted separation of aptamer-functionalized Fe3O4 magnetic nanoparticles and BaYF5:Yb,Er nanoparticles as upconversion fluorescence labels. Talanta 170:350–357. https://doi.org/10.1016/j.talanta.2017.04.021
14. Tsukakoshi K, Abe K, Sode K, Ikebukuro K (2012) Selection of DNA aptamers that recognize α-synuclein oligomers using a competitive screening method. Anal Chem 84:5542–5547. https://doi.org/10.1021/ac300330g
15. Toh SY, Citartan M, Gopinath SCB, Tang T-H (2015) Aptamers as a replacement for antibodies in enzyme-linked immunosorbent assay. Biosens Bioelectron 64:392–403. https://doi.org/10.1016/j.bios.2014.09.026
16. Li J, Guo S, Wang E (2012) Recent advances in new luminescent nanomaterials for electrochemiluminescence sensors. RSC Adv 2(9):3579-3586. https://doi.org/10.1039/C2RA01070D
17. Liu YL, Zhao XJ, Yang XX, Li YF (2013) A nanosized metal–organic framework of Fe-MIL-88NH2 as a novel peroxidase mimic used for colorimetric detection of glucose. Analyst 138(16):4526–4531. https://doi.org/10.1039/C3AN00560G
18. Sun Z, Liu Y, Li Y (2015) Selective recognition of 6-mercaptopurine based on luminescent metal–organic frameworks Fe-MIL-88NH2. Spectrochim Acta A Mol Biomol Spectrosc 139:296–301. https://doi.org/10.1016/j.saa.2014.12.009
19. Hu M, Wang Y, Yang J, Sun Y, Xing G, Deng R, Hu X, Zhang G (2019) Competitive electrochemical immunosensor for maduramicin detection by multiple signal amplification strategy via hemin@Fe-MIL-88NH2/AuPt. Biosens Bioelectron 142:111554. https://doi.org/10.1016/j.bios.2019.111554
20. Rowsell JLC, Yaghi OM (2004) Metal–organic frameworks: a new class of porous materials. Microporous Mesoporous Mater 73(1):3–14. https://doi.org/10.1016/j.micromeso.2004.03.034
21. Ke F, Qiu L-G, Zhu J (2014) Fe3O4@MOF core–shell magnetic microspheres as excellent catalysts for the Claisen–Schmidt condensation reaction. Nanoscale 6(3):1596–1601. https://doi.org/10.1039/C3NR05051C

22. Zhao S, Zhang Y, Ding S, Fan J, Luo Z, Liu K, Shi Q, Liu W, Zang G (2019) A highly sensitive label-free electrochemical immunosensor based on AuNPs-PtNPs-MOFs for nuclear matrix protein 22 analysis in urine sample. J Electroanal Chem 834:33–42. https://doi.org/10.1016/j.jelechem.2018.12.044
23. Liu L, Zhou Y, Liu S, Xu M (2018) The applications of metal−organic frameworks in electrochemical sensors. ChemElectroChem 5(1):6–19. https://doi.org/10.1002/celc.201700931
24. Li Y, Yu C, Yang B, Liu Z, Xia P, Wang Q (2018) Target-catalyzed hairpin assembly and metal-organic frameworks mediated nonenzymatic co-reaction for multiple signal amplification detection of miR-122 in human serum. Biosens Bioelectron 102:307–315. https://doi.org/10.1016/j.bios.2017.11.047
25. Xie S, Ye J, Yuan Y, Chai Y, Yuan R (2015) A multifunctional hemin@metal–organic framework and its application to construct an electrochemical aptasensor for thrombin detection. Nanoscale 7(43):18232-18238. https://doi.org/10.1039/C5NR04532K
26. Cheng S, Liu H, Zhang H, Chu G, Guo Y, Sun X (2020) Ultrasensitive electrochemiluminescence aptasensor for kanamycin detection based on silver nanoparticle-catalyzed chemiluminescent reaction between luminol and hydrogen peroxide. Sensors Actuators B Chem 304:127367. https://doi.org/10.1016/j.snb.2019.127367
27. Chen F, Wang D, Chen J, Ling J, Yue H, Gou L, Tang H (2020) PtNi nanocubes-catalyzed tyramine signal amplification electrochemiluminescence sensor for nonenzymatic and ultrasensitive detection of hepatocellular carcinoma cells. Sensors Actuators B Chem 305:127472. https://doi.org/10.1016/j.snb.2019.127472
28. Chen Y, Zhou S, Li L, Zhu J-j (2017) Nanomaterials-based sensitive electrochemiluminescence biosensing. Nano Today 12:98–115. https://doi.org/10.1016/j.nantod.2016.12.013
29. Zhang Y, Wei Q (2016) The role of nanomaterials in electroanalytical biosensors: a mini review. J Electroanal Chem 781:401–409. https://doi.org/10.1016/j.jelechem.2016.09.011
30. Liu YL, Fu WL, Li CM, Huang CZ, Li YF (2015) Gold nanoparticles immobilized on metal–organic frameworks with enhanced catalytic performance for DNA detection. Anal Chim Acta 861:55–61. https://doi.org/10.1016/j.aca.2014.12.032
31. Xie S, Ye J, Yuan Y, Yaqin C, Yuan R (2015) A multifunctional hemin@metal-organic framework and its application to construct an electrochemical aptasensor for thrombin detection. Nanoscale 7:18232–18238. https://doi.org/10.1039/c5nr04532k
32. Wang X, Zhai S, Liu C, Wang X, Yang Y, Tu Y (2019) A convenient electrochemiluminescent immunosensor for detecting methamphetamine antibody. Anal Sci 35(8):875-882. https://doi.org/10.2116/analsci.19P051
33. Tsukakoshi K, Abe K, Sode K, Ikebukuro K (2012) Selection of DNA aptamers that recognize α-synuclein oligomers using a competitive screening method. Anal Chem 84(13):5542-5547. https://doi.org/10.1021/ac300330g
34. Kasai T, Tokuda T, Taylor M, Kondo M, Mann DMA, Foulds PG, Nakagawa M, Allsop D (2013) Correlation of Aβ oligomer levels in matched cerebrospinal fluid and serum samples. Neurosci Lett 551:17-22. https://doi.org/10.1016/j.neulet.2013.06.029